Discover Oncology

Research

Dissecting PTPN7-driven aggressiveness in IDH-wildtype astrocytomas: multi-omics, clinical validation, and spatial transcriptomics for prognostic insights

Tung Liu[1] · Yu-Chieh Lin[2,3] · Pei-Chi Chang[4] · Dueng-Yuan Hueng[5] · Yao-Feng Li[1,3,4]

Received: 14 February 2025 / Accepted: 10 May 2025
Published online: 24 May 2025

Abstract

Background Gliomas, particularly IDH-wildtype astrocytomas, remain highly aggressive and resistant to current therapies. Despite advances in molecular classification, effective therapeutic targets are still limited. Consequently, identifying new targets is essential to improve patient survival. PTPN7, a tyrosine phosphatase implicated in MAPK signaling, is known to play roles in various malignancies but remains underexplored in gliomas. This study examines the prognostic significance, spatial distribution, and immune-related functions of PTPN7, aiming to elucidate its potential as a prognostic role and therapeutic target in glioma treatment.

Materials and methods We analyzed PTPN7 mRNA expression in gliomas via TCGA, CGGA, and single-cell RNA sequencing (GSE131928 and GSE89567). Kaplan determined prognostic significance–Meier and uni-/multi-variate Cox survival analyses. Gene set enrichment analysis (GSEA) was used to identify dysregulated pathways, immune signatures, and cell-type enrichments. We also applied CIBERSORT to evaluate the relationships between PTPN7 expression and 12-principal cell states and 22 immune populations. Spatial transcriptomics (Ivy Glioblastoma Atlas, 10 × Genomics Visium) mapped PTPN7 distribution; these findings were corroborated by immunohistochemistry-validated protein expression in 70 cases.

Results Pan-cancer analysis revealed PTPN7 overexpression in multiple malignancies, including glioma. Notably, PTPN7 was significantly elevated in IDH-wildtype astrocytomas, correlating with higher tumor grades and poorer overall survival. GSEA indicated that high PTPN7 is linked to T-cell differentiation, macrophage/monocyte activation, and dendritic cell-associated pathways. Both immune deconvolution and single-cell analyses showed that PTPN7 positively correlates with myeloid series and T-cell populations, supported by additional GSEA findings. In the Ivy dataset and spatial transcriptomics, PTPN7 was concentrated in peri-necrotic, cellular tumor, and slightly lower in the infiltrating border regions, consistent with immune interaction sites. Immunohistochemical data further demonstrated high PTPN7 expression tracks with increased tumor grade, reaching statistical significance in IDH-wildtype astrocytomas and confirming its clinical relevance.

Conclusion This study positions PTPN7 as a prognostic biomarker and immune modulator in gliomas, particularly IDH-wildtype astrocytomas. Its expression correlates with tumor aggressiveness and immune infiltration, potentially driving

Supplementary Information The online version contains supplementary material available at https://doi.org/10.1007/s12672-025-02662-5.

✉ Yao-Feng Li, liyaofeng1109@gmail.com | [1]Department of Pathology, Tri-Service General Hospital, National Defense Medical Center, Taipei 114, Taiwan, Republic of China. [2]Department of Pathology and Laboratory Medicine, Taoyuan Armed Forces General Hospital, Taoyuan 325, Taiwan, Republic of China. [3]Graduate Institute of Medical Sciences, National Defense Medical Center, Taipei 114, Taiwan, Republic of China. [4]Graduate Institute of Life Sciences, National Defense Medical Center, Taipei 114, Taiwan, Republic of China. [5]Department of Neurologic Surgery, Tri-Service General Hospital, National Defense Medical Center, Taipei, Taiwan, Republic of China.

glioma progression. Targeting PTPN7 may disrupt immune evasion and support tumor eradication, indicating a promising therapeutic avenue in immunotherapy-based strategies.

Keywords PTPN7 · Glioma · Glioblastoma · TCGA · CGGA · Ivy dataset · GSEA · Spatial transcriptomes · Single-cell sequencing · CIBERSORT

Abbreviations

CGGA	Chinese Glioma Genome Atlas
CIBERSORT	Cell-type Identification by Estimating Relative Subsets of RNA Transcripts
CT	Chemotherapy
EGFR	Epidermal growth factor receptor
ERK	Extracellular signal-regulated kinase
GBM	Glioblastoma
GEO	Gene Expression Omnibus
GEPIA	Gene Expression Profiling Interactive Analysis
GSEA	Gene Set Enrichment Analysis
HePTP	Hematopoietic Protein Tyrosine Phosphatase
KPS	Karnofsky Performance Score
LGG	Lower-grade glioma
PD-L1	Programmed death-ligand 1
PDC	Proteomic Data Commons (TCGA)
PI3K	Phosphoinositide 3-kinase
PTPN7	Protein tyrosine phosphatase non-receptor type 7
RPKM	Reads per kilobase per million
RT	Radiotherapy
TAM	Tumor-associated macrophage
TCGA	The Cancer Genome Atlas
TERT	Telomerase reverse transcriptase
TMZ	Temozolomide
TPM	Transcripts per million
UMAP	Uniform Manifold Approximation and Projection
VEGF	Vascular endothelial growth factor

1 Background

Primary brain tumors, particularly gliomas, account for a major proportion of central nervous system malignancies worldwide. According to the latest epidemiological reports, glioblastoma (GBM) alone represents the most frequently diagnosed and lethal subtype among diffuse gliomas, which overall constitute approximately two-thirds of malignant primary brain tumors [1]. Over the past 15 years, the classification of gliomas has advanced significantly. The 2007 World Health Organization (WHO) guidelines primarily relied on classic histopathological characteristics—such as cellular atypia, mitotic rate, microvascular proliferation, and tumor necrosis—to stratify astrocytomas, oligodendrogliomas, and glioblastomas into grades II, III, or IV [2]. A paradigm shift occurred in 2016 when the WHO incorporated key molecular parameters, most notably IDH1/2 mutations and 1p19q co-deletion status [3], to distinguish IDH-mutant astrocytomas from oligodendrogliomas (IDH-mutant with 1p19q co-deletion) and IDH-wildtype glioblastomas. The 2021 WHO classification [4] has refined this approach further, emphasizing additional markers such as TERT promoter mutations [5], EGFR amplification [5], chromosome 7/10 alterations [5], and MGMT promoter methylation status [6] for IDH-wildtype astrocytomas, and CDKN2A/B deletions [7] for IDH-mutant astrocytoma. This molecular classification greatly aids personalized diagnostic and therapeutic strategies in clinical neuro-oncology. Standard-of-care for high-grade glioma typically involves maximal safe surgical resection, followed by radiotherapy and temozolomide (TMZ) chemotherapy [8]. Although this approach modestly extends median survival to around 14.6 months in GBM

[9], the prognosis remains grim, with high recurrence rates. Variations in MGMT promoter methylation status significantly affect response to TMZ, leading to therapy resistance in many patients [6]. Additionally, research by Professor Luis F. Parada and others has shown that glioblastomas harbor quiescent and proliferative stem-like cell populations capable of escaping cytotoxic agents, further driving relapse [10].

Over the past decades, extensive research has focused on discovering new therapeutic targets for brain tumors involving RTK, PI3K, and VEGF inhibitors. Despite numerous clinical trials, the outcomes have largely exceeded expectations [11]. Therefore, pursuing novel targets remains essential to broadening available chemotherapeutic strategies [12–16]. However, bioinformatic tools like GEPIA [17, 18], UCSC Xena [19], and cBioPortal [20] have facilitated large-scale gene expression analyses. Still, they often rely on older tumor classifications or sometimes sub-optimal transcriptome units, Reads per kilobase per million (RPKM), which causes bias when screening the biomarker between samples. These limitations can obscure marker discovery, especially in a setting as complex as glioma. To address this issue, we integrated raw data from multiple consortia (TCGA, CGGA) for sophisticated bioinformatics with updated tumor classification and proper transcriptome unit "transcripts per million, TPM," employing multivariate prognostic factor screening to identify potential therapeutic targets. Additionally, we integrated advanced computational approaches (CIBERSORT, single-cell analysis, spatial transcriptomics) to systematically identify overlooked targets in a subtype- and region-specific manner. From our analyses and literature reviews, we noticed that Protein tyrosine phosphatase non-receptor gene family (PTPN**,** also known as HePTP) have been showed prognostic and therapeutic role [21–24]. Protein tyrosine phosphatase non-receptor type 7 (PTPN7**,** also known as HePTP) is one of them, known for dephosphorylating MAPK family members such as ERK, p38, and JNK in hematopoietic and immune cells [25]. Dysregulated MAPK signaling is implicated in numerous malignancies, making phosphatases like PTPN7 intriguing yet underexplored. Over the past few years, multiple lines of evidence support the notion that PTPN7 is elevated in various malignancies, including non-small-cell lung cancer [26], leukemia [27], melanoma [28], breast cancer [29], and bladder cancer [25]. Building upon previous findings that suggested a potential immunomodulatory role for PTPN7 in gliomas [24], our study advances this understanding by incorporating the latest 2021 WHO classification, comprehensive immune genesets analyses using GSEA through cancer hallmark/immune/cell-type genesets, integrated spatial and single-cell transcriptomic analyses, as well as 70 clinical tissue validation to provide a more detailed characterization of the PTPN7 prognostic and therapeutic roles in the glioma.

2 Materials and methods

2.1 Data collection for bioinformatics analyses

This study drew upon five datasets to investigate PTPN7 expression and its clinical relevance. (1) Primary Bioinformatics Cohort (TCGA): We obtained the transcriptomic (mRNA) profiles and associated clinical information (gender, age, histology, tumor grade, overall survival, and vital status) from The Cancer Genome Atlas (TCGA; https://portal.gdc.cancer.gov/). A total of 690 glioma cases were initially included under an older classification scheme; these were subsequently reclassified according to the 2021 WHO system into three main subgroups: IDH wildtype, IDH mutant astrocytoma, and oligodendroglioma. (2) Proteomics Dataset (TCGA PDC): To validate transcript-level findings at the protein level, we analyzed the Proteomic Data Commons (TCGA PDC) resource (https://proteomic.datacommons.cancer.gov/pdc/, retrieved Nov. 2024). This dataset comprised 110 proteomic samples (100 glioblastomas and 10 normal controls) with clinical details, including patient age, gender, diagnosis, and tumor grade. (3) Tumor Heterogeneity and Immune Cell Analyses (TCGA and CGGA): For further exploration of tumor heterogeneity and immune infiltration, we utilized both TCGA and the Chinese Glioma Genome Atlas (CGGA; http://www.cgga.org.cn/, retrieved Nov. 2024). (4) Ivy Glioblastoma Atlas: We then examined the Ivy Glioblastoma Atlas Project dataset (https://glioblastoma.alleninstitute.org/), which includes 122 samples derived from 10 patients and 5 heterogeneous tumor regions (leading edge, infiltrating border, cellular tumor, microvascular proliferation, and pseudopalisading necrosis) to evaluate PTPN7 expression patterns. (5) Single-Cell Sequencing: Finally, two single-cell sequencing datasets from the Gene Expression Omnibus (GEO) were employed: one for IDH wildtype gliomas (GSE131928; https://www.ncbi.nlm.nih.gov/geo/query/acc.cgi?acc=GSE131928, retrieved Nov. 2024) and another for IDH mutant gliomas (GSE89567; https://www.ncbi.nlm.nih.gov/geo/query/acc.cgi?acc=GSE89567, retrieved Nov. 2024).

2.2 Transcriptome, proteomics, and single-cell sequencing data processing

We conducted all bioinformatics analyses using R (version 4.1.0; www.r-project.org) and associated packages. The downloaded gene expression files, provided in reads per kilobase per million (RPKM), were converted into transcripts per million (TPM). The *ggpubr* and *limma* packages facilitated mRNA regression analyses and identification of differentially expressed genes (adjusted $p < 0.05$). Next, we performed Kaplan–Meier survival assessments and Cox proportional-hazards modeling to examine the prognostic impact of PTPN7. Single-cell sequencing analyses of GSE131928 and GSE89567 were carried out on the BBrowser platform [30].

2.3 Gene set enrichment analysis (GSEA)

We applied Gene Set Enrichment Analysis (GSEA; https://www.gsea-msigdb.org/gsea/index.jsp, accessed Nov. 2024) [31] to detect pathway alterations between high- and low-PTPN7 expression (defined by the median cutoff) in the TCGA glioma dataset. For this purpose, the (1) H: hallmark gene sets (h.all.v2024.1.Hs.symbols.gmt), (2) C7: immunologic signature gene sets (c7.immunesigdb.v2024.1.Hs.symbols.gmt), and C8: cell type signature gene sets (c8.all.v2024.1.Hs.symbols.gmt) were used as the reference (accessed Nov. 2024), while all other parameters remained at default settings.

2.4 Twelve-cell state and CIBERSORT analyses

To characterize the cellular composition of gliomas, we applied two complementary deconvolution methodologies. Twelve-cell state analysis, developed by Verhaak [32], identifies 12 principal cell types within bulk tumor samples, whereas CIBERSORT (https://cibersort.stanford.edu/) [33] quantifies the relative abundance of 22 immune cell populations from mixed gene expression data. We inputted transcriptomic profiles from the TCGA, CGGA, and Ivy datasets. We calculated the proportion of these 12 cell states and 22 immune cells for each sample, applying a significance threshold of $p < 0.05$. We subsequently examined correlations between PTPN7 expression and each cell type's abundance.

2.5 Tissue microarray and immunohistochemistry

A human glioma tissue microarray (GL1001a) was obtained from Biomax, Inc. (https://www.biomax.us/), providing tissue sections and associated clinical data. All human specimens were collected under informed consent. The array included 59 glioma samples (6 Grade 1, 36 Grade 2, 8 Grade 3, and 9 Grade 4) alongside 11 normal brain tissues; each core was 1.5 mm in diameter and 5 µm thick. To ensure consistent staining, we employed a Ventana Benchmark® XT immunostainer. Following deparaffinization, formalin-fixed sections underwent antigen retrieval in a pressure cooker at 125 °C for 30 min (0.01 M sodium citrate, pH 6.2), followed by three 5-min washes in PBS. The slides were then loaded onto the autostainer according to the manufacturer's protocols. Primary antibodies included PTPN7 (Proteintech #15286-1-AP), KI67 (Abcam #ab15580), and P53 (Cell Signaling #2524). Detection was performed using the Roche Diagnostics OptiView DAB IHC Detection Kit. Both positive and negative controls were processed similarly, confirming antibody specificity.

2.6 Scoring of the immunohistochemistry

Immunohistochemically stained slides were evaluated using semi-quantitative methods adapted from previous studies [12–14]. First, digitized whole-slide images were exported as TIFF files at 10 × magnification. We utilized ImageJ Fiji software (https://imagej.net/software/fiji/downloads) with custom macro scripts to automatically measure the entire tissue area and count positively stained cells (i.e., those showing specific immunoreactivity). The ratio of positive cells per total tissue area (in pixels^2) was then calculated, and the resulting PTPN7 immunostaining density score = 10^5 × (positive cells/pixels^2) was compared against clinical parameters by one-way ANOVA.

2.7 Spatial transcriptome data

To visualize PTPN7 expression in a spatial context, we examined a publicly available 10 × Genomics Visium dataset of an adult glioblastoma (https://www.10xgenomics.com/datasets/human-glioblastoma-whole-transcriptome-analy

sis-1-standard-1-2-0). This sample encompassed approximately 3468 spots, each capturing thousands of transcripts. A log2-transformed PTPN7 expression map was generated, revealing distinct patterns near the necrotic regions, perinecrotic zones, cellular tumor area, infiltrating border, and leading edge.

3 Results

3.1 PTPN7 is upregulated across multiple cancers, including gliomas

A pan-cancer analysis of the TCGA dataset demonstrated a widespread upregulation of PTPN7 across multiple malignancies (Fig. 1A). PTPN7 mRNA expression was significantly higher in tumor tissues (red) compared to their normal counterparts (blue) across various cancer types. Notably, PTPN7 was markedly elevated in several malignancies, including breast invasive carcinoma (BRCA*), cholangiocarcinoma (CHOL***), colon adenocarcinoma (COAD*), esophageal carcinoma (ESCA**), head and neck squamous cell carcinoma (HNSC***), kidney renal clear cell carcinoma (KIRC***), liver hepatocellular carcinoma (LIHC***), lung adenocarcinoma (LUAD***), skin cutaneous melanoma (SKCM***), stomach adenocarcinoma (STAD***), as well as lower-grade glioma (LGG) and glioblastoma (GBM***). The expanded view (Fig. 1B) further substantiates these findings, revealing significant PTPN7 overexpression in GBM (n = 153) and LGG (n = 516) relative to normal brain tissue (n = 5). In contrast, certain malignancies, including kidney chromophobe carcinoma (KICH*),

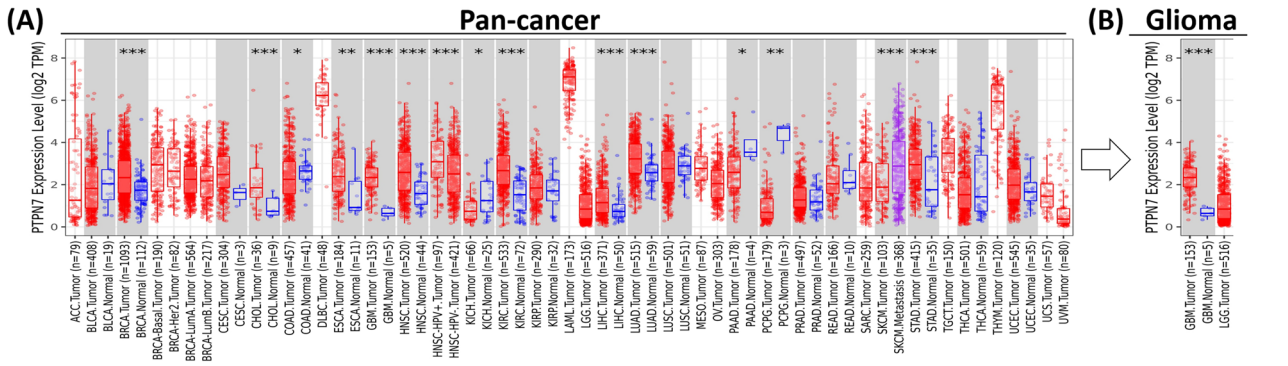

		N	Mean	S.D.	S.E.	95% CI		Min	Max
						Lower limit	Upper limit		
Grade 2	Oligodendroglioma	101	0.563	0.672	0.067	0.430	0.695	.037	4.166
	IDHmu Astrocytoma	124	1.169	1.301	0.117	0.938	1.401	.041	9.177
	IDHwt Astrocytoma	14	1.384	1.461	0.390	0.541	2.228	.087	5.103
	Total	239	0.926	1.132	0.073	0.781	1.070	.037	9.177
Grade 3	Oligodendroglioma	81	0.782	0.966	0.107	0.569	0.996	.011	4.851
	IDHmu Astrocytoma	101	1.945	2.040	0.203	1.542	2.348	.186	16.712
	IDHwt Astrocytoma	11	3.649	3.060	0.922	1.594	5.705	.259	10.224
	Total	193	1.554	1.904	0.137	1.284	1.824	.011	16.712
Grade 4	IDHmu Astrocytoma	22	1.872	1.669	0.356	1.132	2.612	.180	6.259
	IDHwt Astrocytoma	208	4.419	2.710	0.188	4.049	4.790	.119	14.730
	Total	230	4.176	2.731	0.180	3.821	4.530	.119	14.730

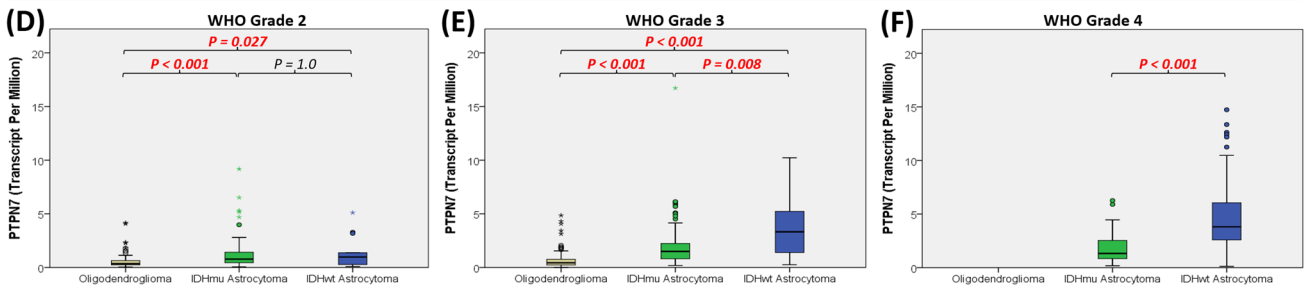

Fig. 1 Pan-cancer analysis of PTPN7 in tumor versus normal across multiple cancer types. **A** Each box represents the 25th–75th percentiles, with the median indicated by a horizontal line, with dots showing data spread. Significance levels (*p < 0.05, **p < 0.01, ***p < 0.001) are noted above each comparison. **B** To the right, an inset compares GBM (n = 153, red) and LGG (n = 516, red) to normal brain samples (n = 5, blue), highlighting marked PTPN7 upregulation in gliomas, particularly in GBM. **C** Summary statistics (N, mean, SD, and 95% CI) of PTPN7 TPM by WHO grade and subtype (oligodendroglioma, IDH-mutant astrocytoma, IDH-wildtype astrocytoma). **D**–**F** Box plots showing PTPN7 distribution split by molecular subgroup within each WHO grade

pancreatic adenocarcinoma (PAAD*), and pheochromocytoma/paraganglioma (PCPG**), exhibited an inverse trend with lower PTPN7 expression in tumors compared to normal tissues. To investigate the role of PTPN7 expression in the glioma, we separated the pan-glioma samples by both WHO grade [2–4], then evaluated the PTPN7 expression to the molecular subtype (oligodendroglioma, IDH-mutant astrocytoma, IDH-wildtype astrocytoma). The results are shown in (Fig. 1C–F). Overall, PTPN7 expression rose with advancing grade, especially in IDH-wildtype tumors. In Grade 2 (Fig. 1D), oligodendrogliomas displayed the lowest average PTPN7, while IDH-mutant astrocytomas had moderately higher levels (1.17 TPM). IDH-wildtype astrocytomas showed further increases (1.38 TPM), though the sample size was small. In Grade 3 (Fig. 1E), PTPN7 remained lowest in oligodendrogliomas (0.78 TPM) but increased substantially in IDH-mutant astrocytomas (1.95 TPM, $p < 0.001$). IDH-wildtype astrocytomas reached a mean of 3.65 TPM ($p < 0.001$), nearly double that of the IDH-mutant group. Among Grade 4 tumors (Fig. 1F), IDH-mutant astrocytomas averaged 1.87 TPM, while IDH-wildtype tumors were highest at 4.42 TPM ($p < 0.001$, Fig. 3D). The box plots confirm these trends: oligodendrogliomas consistently show minimal PTPN7 expression, IDH-mutant astrocytomas occupy an intermediate range, and IDH-wildtype astrocytomas exhibit significantly elevated PTPN7, notably at higher grades.

3.2 PTPN7 is elevated in IDH-wildtype gliomas and predicts poor survival

To further dissect PTPN7 expression across the updated glioma classification, we categorized the pan-glioma cohort into three primary groups: IDH wildtype, IDH mutant astrocytoma, and oligodendroglioma. When comparing PTPN7 expression in tumor versus normal tissues (Figs. 2A–D), a significant difference was observed for the IDH wildtype group but not for the other groups, including the overall pan-glioma comparison. This finding suggests that differences in PTPN7 expression may be masked when IDH wildtype and IDH mutant tumors are evaluated together, as the mutant and oligodendroglioma subgroups do not show the same differential expression. When using the median as a cutoff, high PTPN7 expression correlates with poorer overall survival in the entire glioma cohort (Fig. 2E) and IDH-wildtype astrocytomas (Fig. 2F) in Kaplan–Meier survival curves (Fig. 2E–H). To account for potential confounders in survival analysis, we performed Uni/multi-Cox survival regression (Fig. 2I–L), incorporating clinical covariates such as tumor grade, age, gender, Karnofsky performance score (KPS), radiotherapy (RT), and chemotherapy (CT). The results underscore PTPN7 as a potential prognostic factor in pan-glioma and IDH-wildtype astrocytomas (Fig. 2I, J, Supplementary 1). Finally, to further examine the association between PTPN7 expression and tumor grading, we observed that PTPN7 levels increase with advancing grade (Figs. 2M–O) but show no apparent difference in the oligodendroglioma subgroup (Fig. 2P). These findings indicate that elevated PTPN7 expression is enriched in glioma tissues and correlates with higher malignancy and worse overall survival outcomes.

3.3 Integrating meta-analysis, prognostic modeling, and genomic exploration of PTPN7 in glioma

A meta-analysis integrating data from CGGA and TCGA glioma cohorts revealed that high PTPN7 expression correlates with poorer survival (common-effect HR = 1.30, 95% CI 1.16–1.46, $p < 0.001$, Fig. 3A). To further refine prognostic assessments, we developed a nomogram (Fig. 3B) incorporating PTPN7 expression, gender, chemotherapy, age, Karnofsky performance score, tumor grade, and radiotherapy. Each factor contributes points, which sum to a "Total Points" value that predicts overall survival at 1, 3, and 5 years. For instance, ~449 total points translate to ~63% survival at 1 year, 8% at 3 years, and < 2% at 5 years, illustrating the Nomogram's capacity for individualized risk stratification. To explore potential genomic drivers of PTPN7 overexpression, we examined its mutation status in all TCGA glioma cases, identifying only three mutations (Fig. 3C). Further analysis across all glioma subtypes found no recurrent gene mutations linked to elevated PTPN7 (Fig. 3D, E), implying that other regulatory factors likely underlie its upregulation.

3.4 High-PTPN7 tumors exhibit overlapping immune signatures across glioma subtypes

Next, to understand the altered signaling in the High-PTPN7 Tumors, we compared the high-PTPN7 expression versus the lower-PTPN7 group through gene set enrichment analysis (GSEA) at IDH-wildtype astrocytomas, IDH-mutant astrocytomas, and oligodendrogliomas, using ranked lists of genes correlated with PTPN7 expression (Fig. 4A–C). In each panel, the x-axis represents the rank order of genes, while the y-axis illustrates the running enrichment score for each hallmark pathway. There are 21, 19, and 15 upregulated genesets in IDH-wildtype astrocytomas, IDH-mutant astrocytomas, and oligodendrogliomas individually. Notably, the Venn diagram of upregulated gene sets across these three molecular subtypes reveals a substantial overlap, with 14 hallmark pathways shared among

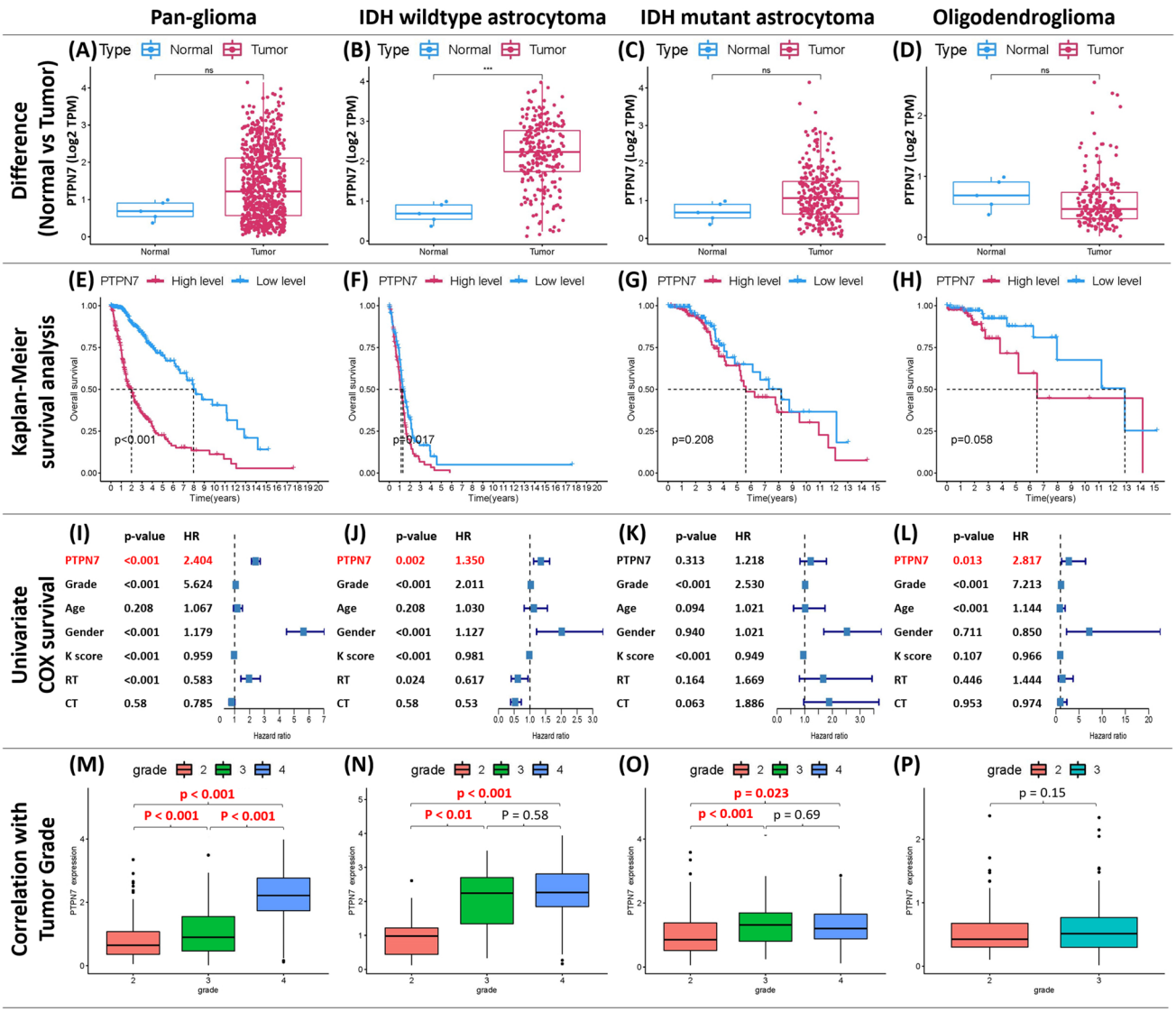

Fig. 2 PTPN7 expression, survival analysis, and grade correlation in gliomas. **A**–**D** Box plots contrasting normal (blue) vs. tumor (pink) PTPN7 expression for pan-gliomas, IDH-wildtype astrocytoma, IDH-mutant astrocytoma, and oligodendroglioma. **E**–**H** Kaplan–Meier curves categorize patients into High (pink) vs. Low (blue) PTPN7 groups, demonstrating worse survival in High expression. **I**–**L** After adjusting for clinical covariates, Cox survival analyses identified PTPN7 as a potential prognostic factor in pan-gliomas, IDH-wildtype astrocytoma, and oligodendroglioma. **M**–**P** Box plots illustrate that PTPN7 increases with advancing glioma grade (**M**–**O**) or remains unchanged in oligodendroglioma (**P**)

them (Fig. 4D), indicating a high degree of commonality in the underlying biological processes, including the ALLOGRAFT_REJECTION, EPITHELIAL_ MESENCHYMAL_TRANSITION, IL2_STAT5_SIGNALING, IL6_JAK_STAT3_SIGNALING, INFLAMMATORY_RESPONSE, INTERFERON_ALPHA_RESPONSE, INTERFERON _GAMMA_RESPONSE, TNFA_SIGNALING_VIA_NFKB, COMPLEMENT, APOPTOSIS, KRAS_SIGNALING_UP, HYPOXIA, P53_PATHWAY, and ANGIOGENESIS. Most of these altered geneset were relevant to the immune response. To further clarify the relationship between PTPN7 and immune reaction, we performed GSEA specifically with immune-focused (C7) and cell-type-based (C8) gene sets, confirming that immune processes are enriched in PTPN7-high gliomas. The number of the relevant genesets in C7 and C8 is shown in (Table 1). Venn diagram (Fig. 4E) highlights that IDH-wildtype tumors have the largest significant genesets associated with high-PTPN7 expression (1510 genesets), while the IDH-mutant (888 genesets) and oligodendroglioma (447 genesets). There were substantial shared regions (435 genes) across different subtypes, and we identified subsets related to T-cell differentiation (151 genes in red), macrophage/monocyte activation (80 in blue), and dendritic cells/antigen presentation (83 in green). These findings underscore high PTPN7 expression correlates

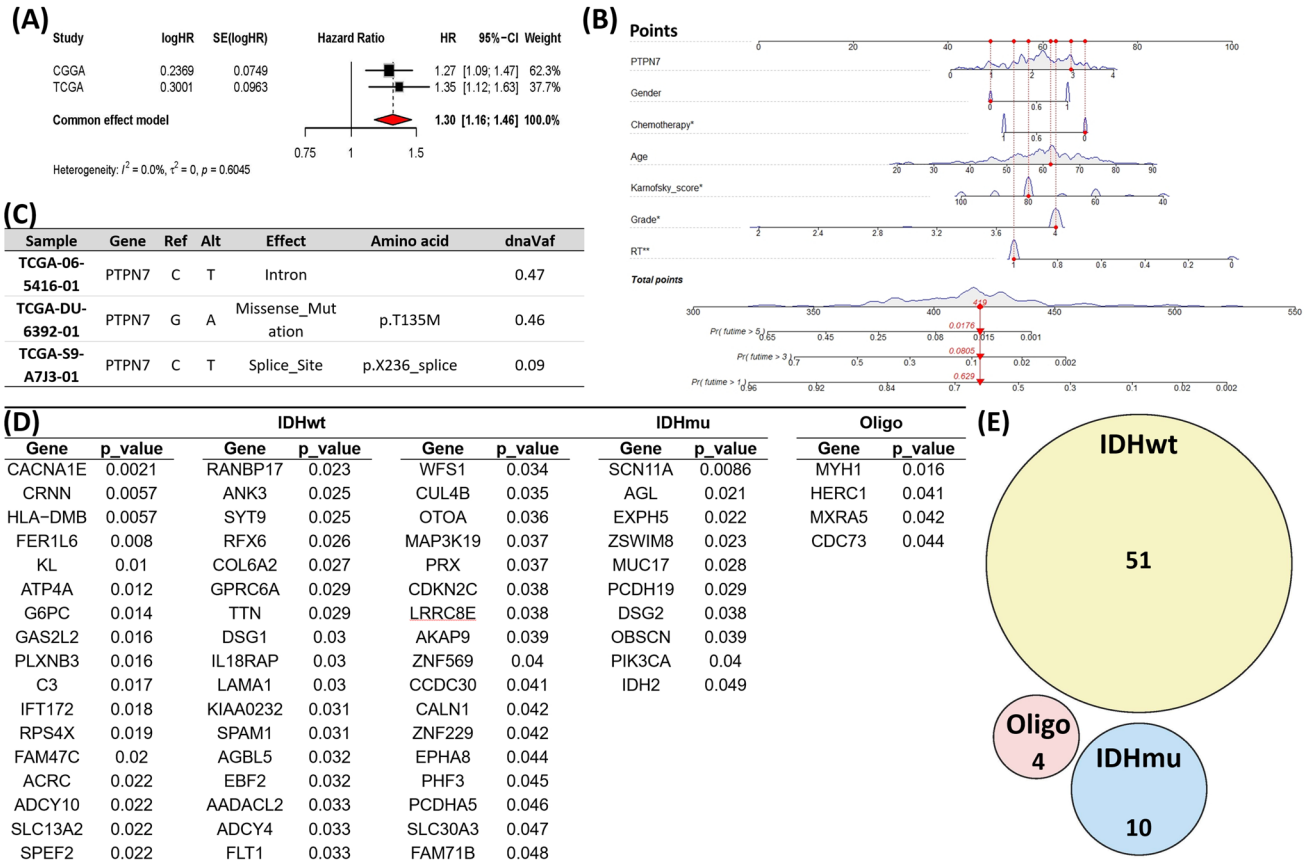

Sample	Gene	Ref	Alt	Effect	Amino acid	dnaVaf
TCGA-06-5416-01	PTPN7	C	T	Intron		0.47
TCGA-DU-6392-01	PTPN7	G	A	Missense_Mutation	p.T135M	0.46
TCGA-S9-A7J3-01	PTPN7	C	T	Splice_Site	p.X236_splice	0.09

IDHwt						IDHmu		Oligo	
Gene	p_value	Gene	p_value	Gene	p_value	Gene	p_value	Gene	p_value
CACNA1E	0.0021	RANBP17	0.023	WFS1	0.034	SCN11A	0.0086	MYH1	0.016
CRNN	0.0057	ANK3	0.025	CUL4B	0.035	AGL	0.021	HERC1	0.041
HLA−DMB	0.0057	SYT9	0.025	OTOA	0.036	EXPH5	0.022	MXRA5	0.042
FER1L6	0.008	RFX6	0.026	MAP3K19	0.037	ZSWIM8	0.023	CDC73	0.044
KL	0.01	COL6A2	0.027	PRX	0.037	MUC17	0.028		
ATP4A	0.012	GPRC6A	0.029	CDKN2C	0.038	PCDH19	0.029		
G6PC	0.014	TTN	0.029	LRRC8E	0.038	DSG2	0.038		
GAS2L2	0.016	DSG1	0.03	AKAP9	0.039	OBSCN	0.039		
PLXNB3	0.016	IL18RAP	0.03	ZNF569	0.04	PIK3CA	0.04		
C3	0.017	LAMA1	0.03	CCDC30	0.041	IDH2	0.049		
IFT172	0.018	KIAA0232	0.031	CALN1	0.042				
RPS4X	0.019	SPAM1	0.031	ZNF229	0.042				
FAM47C	0.02	AGBL5	0.032	EPHA8	0.044				
ACRC	0.022	EBF2	0.032	PHF3	0.045				
ADCY10	0.022	AADACL2	0.033	PCDHA5	0.046				
SLC13A2	0.022	ADCY4	0.033	SLC30A3	0.047				
SPEF2	0.022	FLT1	0.033	FAM71B	0.048				

Fig. 3 The meta-analysis, Nomogram, and Drivers of PTPN7 Expression. **A** A forest plot summarizing hazard ratios (HR) for high PTPN7 expression across the CGGA and TCGA glioma cohorts shows that elevated PTPN7 predicts poorer survival (common-effect HR = 1.30, 95% CI 1.16–1.46, p < 0.001). **B** A nomogram incorporating PTPN7 expression, age, Karnofsky performance score, tumor grade, and treatments assign points to each factor. Higher total points reflect a worse prognosis, and the lower axis indicates corresponding survival probabilities at 1, 3, and 5 years. **C** Analysis of PTPN7 mutations in 690 glioma samples identified only three cases. **D**–**E** No recurrent driver mutations were detected across all glioma subtypes

with broadly recurrent gene set alterations, particularly involving T-cells, macrophages/monocytes, and dendritic cells across multiple glioma subtypes.

3.5 PTPN7-high gliomas show increased myeloid and T-cell proportions

To further investigate cellular populations linked to PTPN7 expression, we analyzed the glioma microenvironment using the modified CIBERSORT technique on bulk RNA-seq data to dissect the 12-key cell populations [32], including tumor (Tumor stem cell, Proliferative tumor stem cell, Differentiated tumor), stromal (Oligodendrocytes, Pericyte, Endothelium, Fibroblast), and immune compartments (Myeloid, Dendritic, Tcell, B cell, and Granulocytes). Table 2 summarizes Spearman correlations between PTPN7 expression and 12 principal cell compartments. The data indicate that PTPN7 expression positively correlates with Myeloid cells, T cells, Granulocytes, and Fibroblasts, suggesting a potential role in shaping the immune and stromal microenvironment. Conversely, negative correlations were observed with stem-like tumors, oligodendrocyte cells, and dendritic cell compartments.

3.6 CIBERSORT analysis links PTPN7 to macrophage and T-cell infiltration

To determine whether immune subpopulations are linked to PTPN7 expression, we analyzed 22 immune cell types estimated by the classical CIBERSORT algorithm [33] in two key datasets, TCGA and CGGA for the investigation. The results indicate that PTPN7 is recurrently positively associated with Macrophages M1 and CD8+ T cells in astrocytomas (Table 3). Other innate immune cells showed sporadic positive associations, including Eosinophils, Neutrophils,

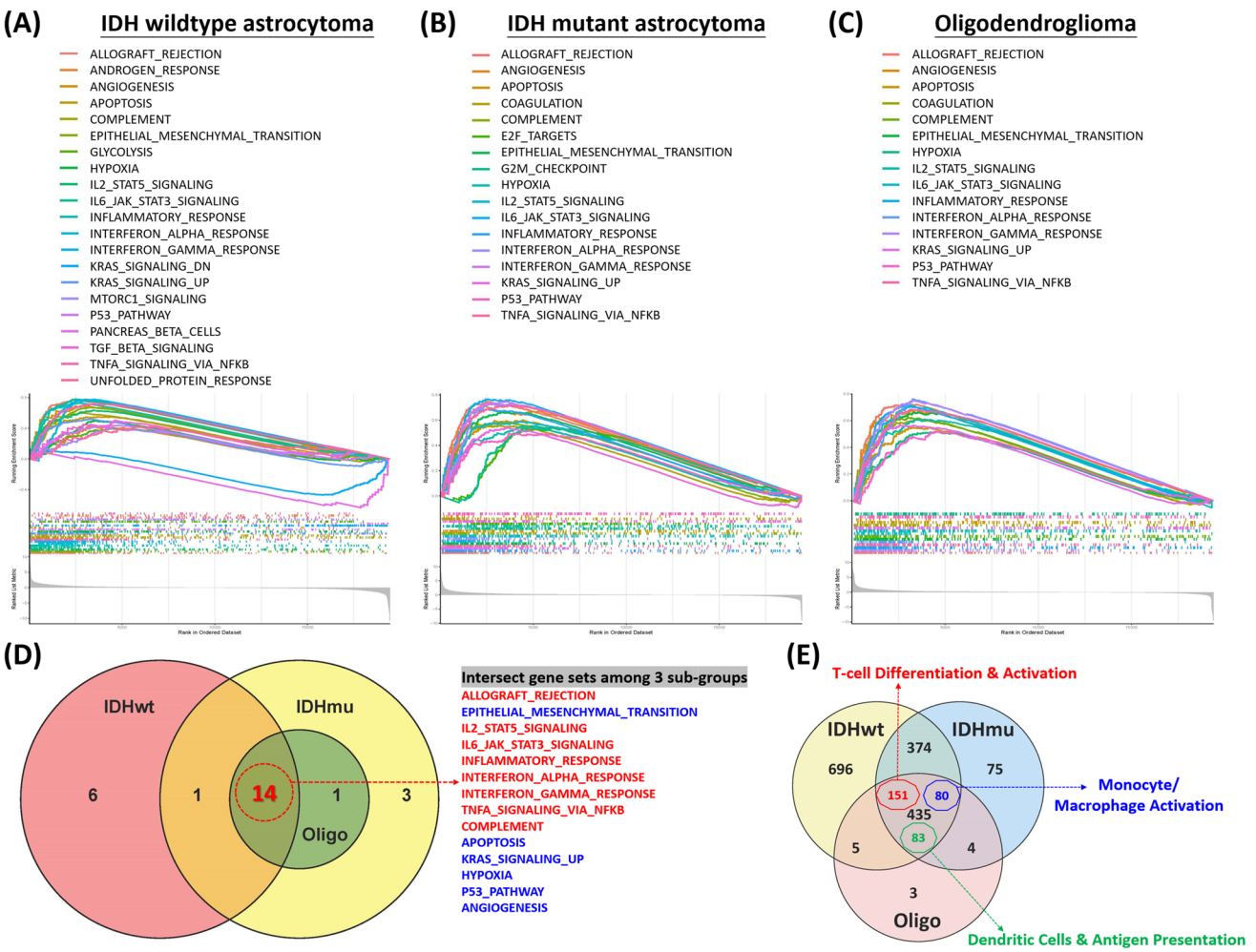

Fig. 4 GSEA results for PTPN7 in three glioma subtypes. **A** IDH-wildtype astrocytoma, **B** IDH-mutant astrocytoma, and **C** oligodendroglioma. Each color traces the running enrichment score of a hallmark gene set (listed at the top). Higher curves indicate stronger enrichment in tumors with high PTPN7. **D** A Venn diagram highlights 14 hallmark sets shared across the three subtypes, underscoring a common immunoinflammatory profile (red text) link with high PTPN7 in gliomas. **E** Venn diagram illustrating immune gene set (C7) overlaps among IDH-wildtype (yellow), IDH-mutant (blue), and oligodendroglioma (pink). Colored numbers highlight T-cell (red), macrophage/monocyte (blue), and dendritic cell (green) subsets across 3-glioma subtypes

Table 1 The number of GSEA with immune-focused (C7) and cell-type-based (C8) gene sets

Category	Immune genesets (C7)	Cell-type genesets (C8)	Total
T-cell Differentiation & Activation	151	24	175
Monocyte/Macrophage Activation	80	34	114
Dendritic Cells & Antigen Presentation	83	11	94
B-cell Mediated Immunity	41	7	48
Neutrophil/Granulocyte Inflammatory	10	4	14
Unclassified	119	122	241

resting NK cells, Gamma-Delta T cells, and T-regulatory (T-reg) subsets. These findings highlight a broader pattern of innate and adaptive immune infiltration in high-PTPN7 tumors, reinforcing the role of PTPN7 in shaping an immunoinflammatory microenvironment. This aligns with previous GSEA findings, further supporting PTPN7's involvement in immune modulation within gliomas.

Table 2 Correlation between PTPN7 expression 12 principal compartments in glioma subtypes

	PTPN7	Datasets	IDH wildtype astrocytoma		IDH mutant astrocytoma		Oligodendroglioma	
		Number (N)	TCGA 233	CGGA 447	TCGA 247	CGGA 352	TCGA 182	CGGA 214
Tumor	Stemcell_tumor	correlation	-.302**	-.330**	-.222**	-.346**	-.345**	-.137*
		p_value	0.000	0.000	0.000	0.000	0.000	0.046
	Prolif_stemcell_tumor	correlation	-0.094	-0.072	0.015	0.018	.309**	-0.061
		p_value	0.154	0.129	0.820	0.737	0.000	0.378
	Differentiated_tumor	correlation	-0.075	-0.059	0.053	.173**	.314**	0.051
		p_value	0.255	0.213	0.406	0.001	0.000	0.460
Stroma	Oligodendrocyte	correlation	-.269**	-.304**	-.154*	-0.074	-0.110	-0.043
		p_value	0.000	0.000	0.016	0.166	0.139	0.533
	Pericyte	correlation	-0.081	0.015	-0.111	0.029	0.021	0.048
		p_value	0.220	0.748	0.081	0.590	0.780	0.485
	Endothelial	correlation	-.140*	-.261**	-0.110	-0.101	0.085	0.077
		p_value	0.033	0.000	0.085	0.059	0.255	0.264
	Fibroblast	correlation	.180**	.433**	.238**	.342**	.471**	.476**
		p_value	0.006	0.000	0.000	0.000	0.000	0.000
Immune	Myeloid	correlation	.694**	.679**	.599**	.555**	.693**	.538**
		p_value	0.000	0.000	0.000	0.000	0.000	0.000
	Dendritic_cell	correlation	-0.097	-.316**	-.235**	-.283**	-.146*	-.196**
		p_value	0.140	0.000	0.000	0.000	0.049	0.004
	T_cell	correlation	.304**	.439**	0.048	.529**	-0.091	.521**
		p_value	0.000	0.000	0.451	0.000	0.220	0.000
	B_cell	correlation	-0.092	0.043	.c	.b	.c	-0.067
		p_value	0.160	0.369				0.329
	Granulocyte	correlation	.521**	.528**	.540**	.432**	.561**	.365**
		p_value	0.000	0.000	0.000	0.000	0.000	0.000

3.7 Proteomics data and immunohistochemistry confirm PTPN7 upregulate in IDH-wildtype gliomas

To validate the bioinformatics analyses derived from the TCGA and CGGA transcriptome datasets, we assessed PTPN7 protein expression using the TCGA proteomic dataset and clinical tissue samples. Proteomic analysis revealed a significantly higher PTPN7 expression in glioblastoma than in normal tissue ($p < 0.001$, Fig. 5A). For clinical validation, we collected 70 clinical cases (including normal brain and IDH-wildtype or IDH-mutant astrocytoma, subdivided by low- vs. high-grade group (Fig. 5B) with PTPN7 immunohistochemical staining. Our data showed that PTPN7 expression was primarily localized in small to medium-sized cells with or without cytoplasmic processes (Fig. 5C, Supplementary 2). Representative tissue microarray cores from H&E staining and low- to high-power IHC illustrate this pattern. Immunoscores ranged from 0.17 (minimal staining) to 48.93 (dense positivity). Box plots (Fig. 5D, E) depict PTPN7 density by WHO grade in IDH-wildtype and IDH-mutant astrocytoma, showing increased expression with higher grades. When comparing normal, low-grade, and high-grade groups, IDH-wildtype high-grade gliomas show the most significant increase in PTPN7 positivity ($p = 0.003$, Fig. 5F). In contrast, IDH-mutant high-grade tumors exhibit no significant difference (Fig. 5G). These findings confirm a strong association between PTPN7 protein expression and glioma progression, particularly in IDH-wildtype, aligning with previous observations (Fig. 2B, F, J).

3.8 Single-cell RNA-Seq reveals PTPN7 enrichment in T cells and myeloid cells

We analyzed single-cell RNA-seq data for IDH-wildtype and IDH-mutant gliomas to validate computational assumptions further. As illustrated in (Fig. 6A–G), analyses were conducted separately for IDH-wildtype gliomas (Fig. 6A–C) and IDH-mutant gliomas (Fig. 6E–G). The UMAP embeddings (Fig. 6A and E) classify cells into broad lineage groups (gray = tumor, blue = T cell, red = glial, yellow = myeloid lineage). In (Fig. 6B and F), a yellow-to-red gradient represents relative PTPN7 expression, with stronger signals detected in T-cell and myeloid populations than in tumor cells. Arrows and arrowheads highlight distinct clusters of T and myeloid cells, respectively. Violin plots (Fig. 6C and G) confirm significant differences in PTPN7 expression among cell types, showing predominant elevation in T-cell and myeloid compartments rather than in malignant or glial cells. These findings align with previous analyses of 12

Table 3 Correlation of PTPN7 expression with 22 immune cell types across glioma subtypes

		IDH wildtype astrocytoma		IDH mutant astrocytoma		Oligodendroglioma	
PTPN7		TCGA	CGGA	TCGA	CGGA	TCGA	CGGA
	n	49	112	86	136	14	24
B_cells_naive	correlation	-0.020	.232*	0.094	0.076	-.596*	.c
	p_value	0.892	0.014	0.391	0.381	0.025	
B_cells_memory	correlation	-0.184	-0.091	-0.057	0.010	0.007	-0.128
	p_value	0.205	0.342	0.605	0.909	0.981	0.551
Plasma_cells	correlation	-0.218	.335**	-0.178	0.139	0.419	0.392
	p_value	0.133	0.000	0.102	0.107	0.136	0.058
T_cells_CD8	correlation	0.138	.283**	0.136	.415**	0.252	.467*
	p_value	0.344	0.002	0.212	0.000	0.385	0.022
T_cells_CD4_naive	correlation	.c	0.026	0.126	-.172*	.c	-0.278
	p_value		0.789	0.247	0.045		0.188
T_cells_CD4_memory_resting	correlation	0.027	-0.001	-.239*	-.275**	0.348	-0.144
	p_value	0.855	0.989	0.027	0.001	0.223	0.502
T_cells_CD4_memory_activated	correlation	0.039	0.073	0.019	0.117	0.423	-0.046
	p_value	0.790	0.446	0.864	0.174	0.132	0.831
T_cells_follicular_helper	correlation	-0.021	-0.078	-0.096	0.016	-0.420	-0.207
	p_value	0.887	0.412	0.378	0.856	0.134	0.332
T_cells_regulatory_Tregs	correlation	0.007	-0.032	-0.145	.308**	-0.266	.477*
	p_value	0.963	0.737	0.183	0.000	0.358	0.018
T_cells_gamma_delta	correlation	.453**	-0.145	-0.038	0.150	0.109	0.124
	p_value	0.001	0.128	0.729	0.081	0.712	0.562
NK_cells_resting	correlation	-0.018	-0.161	0.000	-.263**	-0.298	-0.139
	p_value	0.903	0.090	0.997	0.002	0.301	0.518
NK_cells_activated	correlation	-0.068	-0.007	-0.121	0.154	-0.011	.406*
	p_value	0.643	0.942	0.265	0.073	0.972	0.049
Monocytes	correlation	0.199	-0.055	0.025	-0.126	-.726**	-0.094
	p_value	0.171	0.565	0.823	0.145	0.003	0.664
Macrophages_M0	correlation	-0.275	-0.120	0.094	0.094	.621*	0.142
	p_value	0.056	0.206	0.390	0.276	0.018	0.507
Macrophages_M1	correlation	.412**	0.121	.318**	.281**	0.222	0.180
	p_value	0.003	0.205	0.003	0.001	0.447	0.400
Macrophages_M2	correlation	0.125	-0.127	0.071	0.026	0.308	0.036
	p_value	0.392	0.183	0.518	0.763	0.284	0.868
Dendritic_cells_resting	correlation	0.272	0.018	-0.134	0.041	-0.086	0.167
	p_value	0.058	0.854	0.218	0.639	0.771	0.436
Dendritic_cells_activated	correlation	0.025	-0.013	0.023	-0.009	.c	0.068
	p_value	0.867	0.895	0.835	0.918		0.753
Mast_cells_resting	correlation	-0.145	-0.054	0.079	-0.062	0.093	0.045
	p_value	0.321	0.569	0.468	0.476	0.753	0.835
Mast_cells_activated	correlation	0.008	0.004	-0.076	-.175*	-0.089	-0.395
	p_value	0.957	0.965	0.487	0.042	0.762	0.056
Eosinophils	correlation	0.001	.252**	0.207	-0.104	-0.091	-0.145
	p_value	0.994	0.007	0.056	0.227	0.757	0.499
Neutrophils	correlation	0.173	.230*	0.058	0.067	0.055	-0.242
	p_value	0.234	0.015	0.597	0.437	0.853	0.254

principal cellular populations (Table 2) and CIBERSORT profiling of 22 immune cell types (Table 3), further supporting PTPN7's potential immunoregulatory role within the glioma microenvironment.

3.9 Spatial transcriptomics highlights PTPN7's role in tumor-immune dynamics

In order to better understand the spatial distribution of PTPN7 expression in glioblastoma, a highly heterogeneous tumor, we utilized spatial transcriptomic data from the Ivy Glioblastoma Atlas. This analysis demonstrates how PTPN7 expression varies across five distinct histologic zones: leading edge, infiltrating border, cellular tumor, microvascular proliferation, and pseudopalisading cells around necrosis (Fig. 7A). A notable increase in PTPN7 is observed in the cellular tumor zone ($p = 0.046$) compared to the leading edge (a relatively normal area), followed by microvascular proliferation and pseudo-palisading cells (peri-necrotic region), indicating a potential site of tumor expansion and immune interplay. The correlation table (Fig. 7B) presents Spearman coefficients for PTPN7 expression versus multiple cell fractions using the previous 12 principal cellular deconvolution [32] at Ivy bulk mRNA data. Despite segmented data, we observed a rise in myeloid and fibroblast populations within tumor components, while these populations decreased in the necrotic region, aligning with prior analyses (Table 2). For T cells, a correlation with PTPN7 expression was enormously significant at the leading edge ($r = 0.796$, $p < 0.001$) but became undetectable in the tumor core. These findings suggest that PTPN7 is spatially enriched in highly interactive tumor-immune interfaces, particularly in the cellular tumor zone, where it may influence immune dynamics.

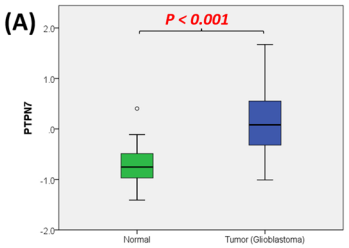

(B)

PTPN7		N	Mean	S.D.	S.E.	95% CI Lower limit	95% CI Upper limit	Min	Max
Normal		11	1.40710	1.546833	.466388	.36792	2.44627	.170	4.595
Low grade	IDH-wildtype	24	6.00606	6.260431	1.277905	3.36251	8.64961	.167	23.827
	IDH-mutant	18	3.55738	5.006987	1.180158	1.06746	6.04730	.412	21.736
High grade	IDH-wildtype	13	14.03098	14.609932	4.052066	5.20228	22.85967	.326	48.935
	IDH-mutant	4	8.67361	13.353864	6.676932	-12.57537	29.92259	.523	28.570
Total		70							

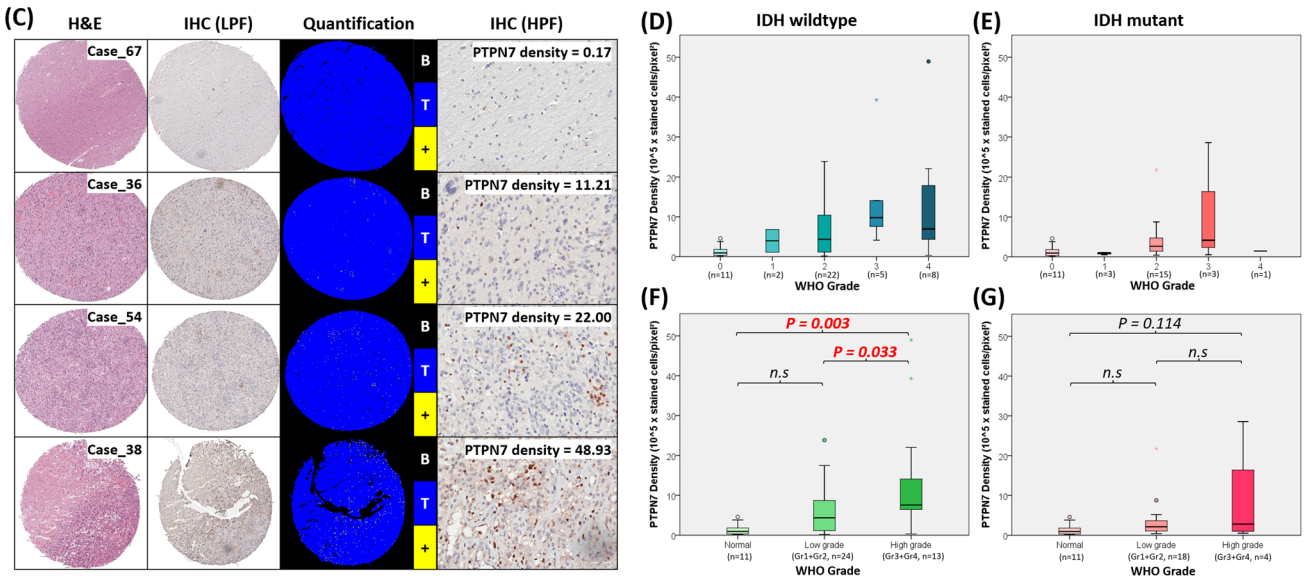

Fig. 5 Immunohistochemical quantification of PTPN7 in normal brain and gliomas. **A** TCGA proteomic analysis confirmed elevated PTPN7 expression in glioblastoma over normal tissue. **B** Summary table of PTPN7 density (mean ± SD) in normal tissue (n = 11) and IDH-wildtype (n = 37) and IDH-mutant glioma (n = 22). **C** Representative tissue cores (H&E, low-power IHC, automated machine quantification, and high-power IHC) reveal immunostaining ranging from 0.17 to 48.93. (Black = background [B], Blue = Tissue [T], Yellow "+" = staining cells). **D**, **E** Box plots of PTPN7 density by WHO grade for IDH-wildtype or IDH-mutant astrocytoma. **F**, **G** Comparisons of normal, low-grade, and high-grade groups. Elevated PTPN7 correlates with tumor grade in the IDH wildtype group but is obscure in the IDH mutant group

3.10 Spatial transcriptomics confirms PTPN7 expression peaks in peri-necrotic and cellular tumor

To examine PTPN7 expression at subregional resolution in glioblastoma, we utilized the 10 × Genomics Visium Whole Transcriptome platform on a human GBM sample (Parent_Visium_Human_Glioblastoma, https://www.10xgenomics.com/datasets/human-glioblastoma-whole-transcriptome-analysis-1-standard-1-2-0). As shown in (Fig. 8A) presents an H&E-stained tissue section with 3468 spots under tissue coverage for Visium transcriptome analyses. Library sequencing achieved an average of 136,128 reads per spot, with a median of 4326 genes detected per spot. Mapping metrics revealed that around 85.4% of reads were confidently mapped to the transcriptome, which was consistent with high-fidelity data (sequencing saturation of 87.3%). The (Fig. 8B) overlays the log2-transformed PTPN7 expression across each spot. Higher PTPN7 signals localize to the peri-necrotic and cellular tumor, whereas lower signals appear along the infiltrating border and leading edges. These spatial patterns reinforce observations from preceding analyses (Fig. 7A), highlighting PTPN7 as a potentially critical immunomodulatory and tumor-associated factor within glioblastoma microenvironments.

4 Discussion

4.1 PTPN7 overexpression and immunomodulatory potential in IDH-wildtype gliomas

Identifying potential targets remains crucial for improving overall survival and expanding chemotherapeutic strategies in glioma patients. We begin by comprehensively analyzing the PTPN gene family, which contains 17 members. From

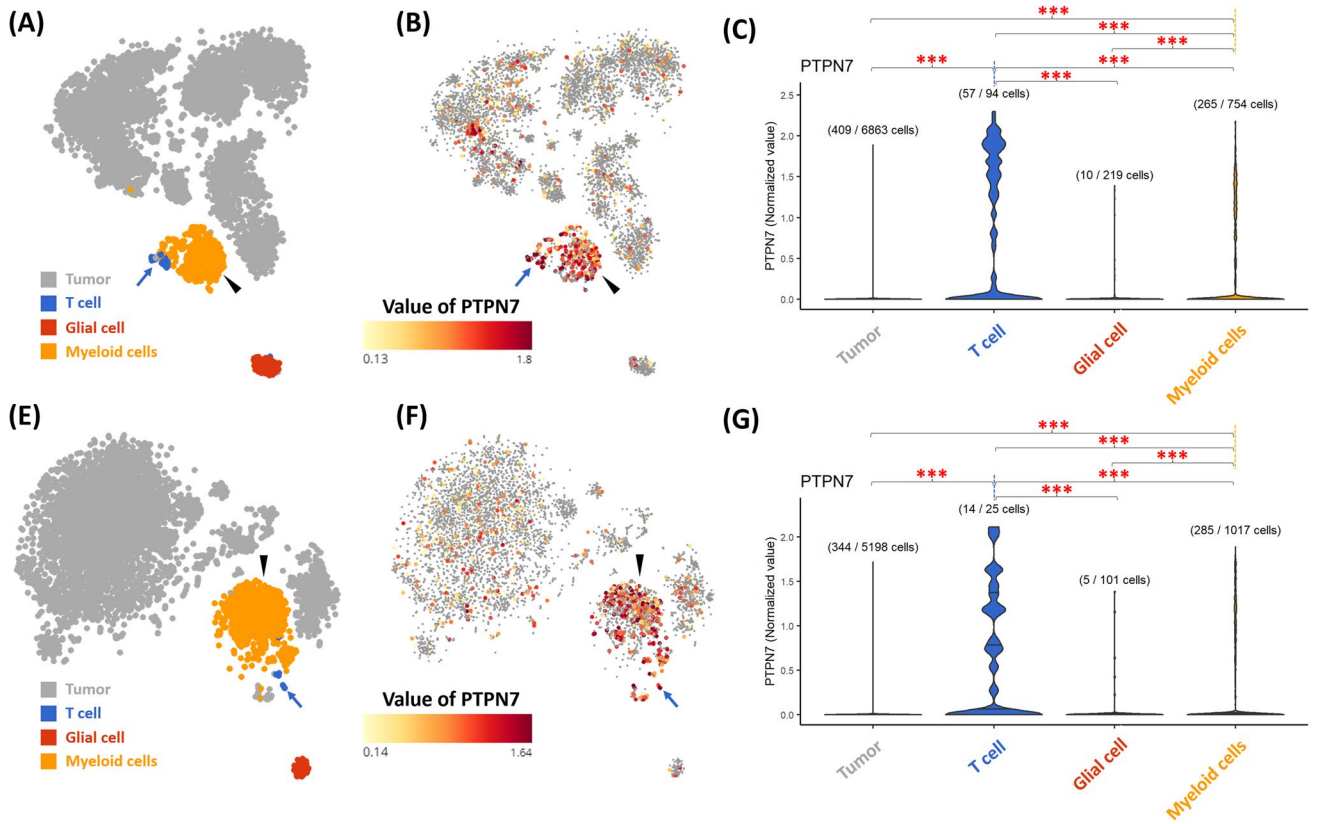

Fig. 6 Single-Cell RNA-Seq Visualization of PTPN7 in IDH-Wildtype (**A**–**C**) and IDH-Mutant (**E**–**G**) Gliomas. UMAP plots (**A**, **E**) color-code cells by major lineage (tumor, T cell, glial, myeloid), while (**B**, **F**) display normalized PTPN7 expression (yellow = low, red = high). Violin plots (**C**, **G**) compare PTPN7 levels across lineages, showing significantly higher expression in T cells (blue) and myeloid cells (orange) (***p < 0.001). Arrows and arrowheads indicate clusters enriched for T or myeloid populations

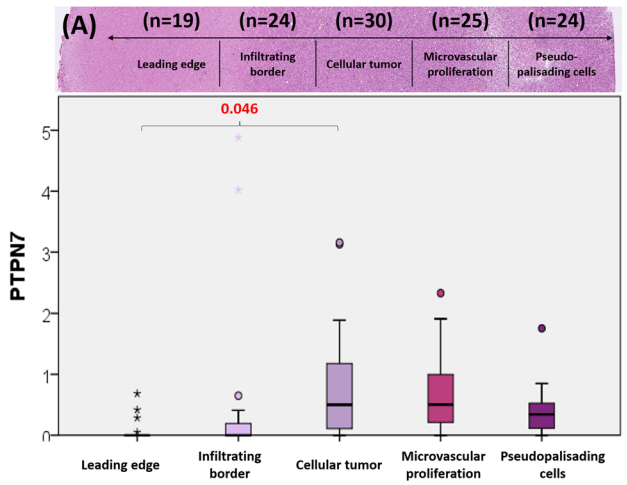

(B)

		Leading Edge (n=19)	Infiltrating border (n=24)	Cellular tumor (n=30)	Microvascular proliferation (n=25)	Pseudopalisading cells (n=24)
Stemcell_tumor	correlation	-0.422	-0.162	-0.232	0.311	-0.142
	p value	0.072	0.449	0.218	0.130	0.507
Prolif_stemcell_tumor	correlation	.477*	0.332	-0.329	-0.004	-0.309
	p value	0.039	0.113	0.076	0.987	0.142
Differentiated_tumor	correlation	0.149	-0.264	0.253	-0.264	0.122
	p value	0.543	0.213	0.177	0.203	0.571
Oligodendrocyte	correlation	-0.233	-0.348	0.004	0.152	-0.063
	p value	0.338	0.096	0.984	0.470	0.771
Pericyte	correlation	-0.089	-0.344	0.319	0.087	0.081
	p value	0.718	0.100	0.086	0.681	0.706
Endothelial	correlation	-0.185	-0.372	0.165	0.110	0.168
	p value	0.448	0.074	0.384	0.602	0.433
Fibroblast	correlation	.582**	-0.091	.449*	-0.100	0.368
	p value	0.009	0.673	0.013	0.634	0.077
Myeloid	correlation	0.236	.665**	0.253	.430*	0.285
	p value	0.330	0.000	0.177	0.032	0.176
Dendritic_cell	correlation	-0.019	-.477*	0.152	0.260	.405*
	p value	0.940	0.018	0.422	0.209	0.050
B_cell	correlation	-0.390	-0.128	-0.282	-0.051	-0.058
	p value	0.099	0.551	0.130	0.809	0.787
T_cell	correlation	.796**	0.133	0.265	-0.146	-0.237
	p value	0.000	0.535	0.157	0.485	0.265
Granulocyte	correlation	0.420	.823**	0.259	-0.207	-0.004
	p value	0.074	0.000	0.167	0.321	0.985

Fig. 7 Spatial Distribution of PTPN7 in Glioblastoma and Its Correlation with Cell Fractions. **A** Box plot of PTPN7 expression (y-axis) across five histologic regions (x-axis): leading edge (n = 19), infiltrating border (n = 24), cellular tumor (n = 30), microvascular proliferation (n = 25), and pseudopalisading cells around necrosis (n = 24). The results showed that PTPN7 is significantly elevated in the cellular tumor zone (p = 0.046) versus the leading edge. **B** Correlation table summarizing Spearman coefficients (and p-values) for PTPN7 expression across various tumor, stromal, and immune cell subsets in each region

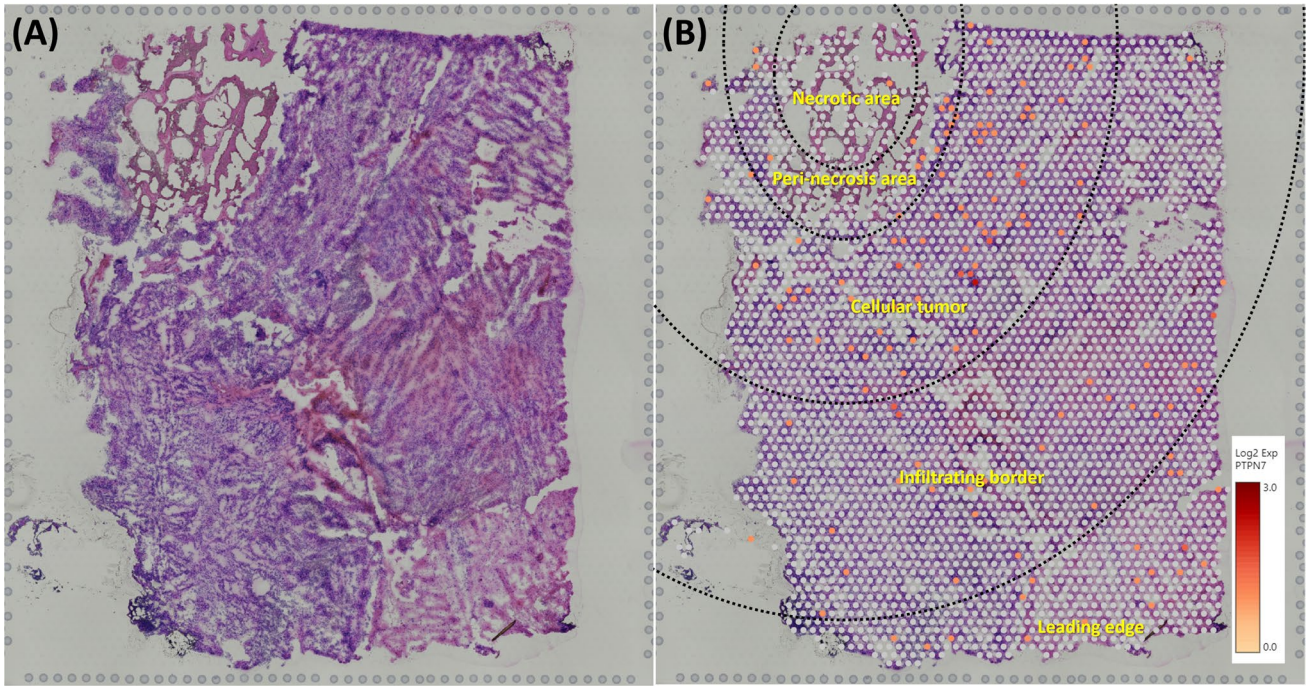

Fig. 8 Spatial transcriptomic profiling of an adult glioblastoma via the 10×Genomics Visium platform. **A** H&E image showing the tissue section. **B** A pseudocolor map of the PTPN7 expression is overlaid in the same section. Key tumor subregions—leading edge, infiltrating border, cellular tumor, peri-necrotic area, and necrotic core—are delineated by dashed lines

the results (Supplementary_1), we identified four potential targets for further exploration: PTPN4, PTPN6, PTPN7, and PTPN11 (Table 4). These markers have also appeared in recent investigations [21–24]. Building on earlier indications of PTPN7's immunomodulatory role in gliomas [24], this study offers key advancements: (1) use of the updated 2021 WHO classification, (2) emphasis on immune geneset analysis through GSEA, (3) integrated spatial and (4) single-cell transcriptomic approaches, and (5) clinical tissue validation, to explore the prognostic and therapeutic implications of PTPN7 in glioma. Our data demonstrate that PTPN7 is overexpressed across multiple malignancies, including glioma. In IDH-wildtype astrocytomas, high PTPN7 correlates with advanced tumor grade, poor survival, and GSEA-identified T-cell, macrophage, and dendritic cell pathways. Immune deconvolution and single-cell analyses verify its positive correlation with macrophages and T cells. Spatial transcriptomics localizes PTPN7 to the peri-necrotic, cellular tumor, and infiltrating border regions. Immunohistochemical analyses confirm elevated PTPN7 in higher-grade IDH-wildtype astrocytomas. In TCGA glioma samples, only three PTPN7 mutations were detected; no repeated driver gene was found across glioma subtypes, suggesting alternative regulatory mechanisms underlie its elevated expression. In the deconversion analyses, we found the fibroblast ratio also correlates with PTPN7 expression. The brain lacks a true fibroblast-rich stroma, so any "fibroblast" signal in glioma likely arises from other mesenchymal components [34]. Such a fibroblast-like signature could reflect reactive stromal changes (e.g. scar-like extracellular matrix deposition) or a partial epithelial-mesenchymal transition of cells in these tumors. In the GSEA cancer hallmark geneset analyses (Fig. 4E), we also noticed that the epithelial-mesenchymal transition was significantly relevant to the high-PTPN7 expression group.

Table 4 Summary of the potential target in the PTPN gene family analyses

	Difference (normal vs. tumor)	*p*-value (KM survival)	*p*-value (uni-COX)	*p*-value (multi-COX)
PTPN4	**	***	***	p = 0.019
PTPN6	**	*	*	p = 0.058
PTPN7	***	**	**	p = 0.078
PTPN11	n.s	**	**	n.s

$p < 0.05$ (*), $p < 0.01$ (**), and $p < 0.001$ (***)

4.2 PTPN7 expression links to the T cell activation, myeloid, and dendritic cells signatures

We identified three major themes by analyzing ImmuneSigDB (C7) and cell-type (C8) collections: T-cell Differentiation & Activation, Monocyte/Macrophage Activation, and Dendritic Cells & Antigen Presentation. First, we observed numerous signatures representing T-cell subsets (e.g., naïve vs. memory $CD4^+$/$CD8^+$ T cells, IL-21/IFN-driven T-cell responses) and cell-type data indicating effector/memory T-cell populations (Supplementary_3). Second, many signatures feature monocyte/macrophage lineage genes induced by TREM1, LPS, or IFN; overlaps in cell-type datasets similarly highlight various monocyte-derived or tissue-resident macrophages (e.g., microglia). Since gliomas commonly harbor abundant tumor-associated macrophages, these findings reinforce a strong myeloid axis linked to PTPN7 upregulation. Third, multiple dendritic cell (DC)-related pathways and cell-type signatures converge on antigen presentation functions. Bulk-mRNA deconvolution and single-cell analyses confirm that PTPN7 is enriched in T cells and myeloid compartments. Recently, the PTPN7 has been implicated in driving M2-like (immunosuppressive) polarization [24], aligning with tumor-promoting macrophage roles often observed in gliomas. However, our data slightly highlight that PTPN7 expression in IDH-wildtype astrocytomas aligns with M1-type macrophage signatures and heightened $CD8^+$ T-cell infiltration (Table 3). One plausible explanation is varying classifications and methodologies across studies—such as different WHO classification schemes. In this study, the PTPN7 is significantly prognostic in the IDH wildtype astrocytoma. We then focus on the PTPN7 immune signature in the IDH wildtype context without intermixing the IDH mutant glioma (including IDH mutant astrocytoma and oligodendroglioma). This may lead to disparate macrophage subset findings. Moreover, the M1/M2 model is increasingly recognized as too simplistic for glioma-associated macrophages, which often exhibit mixed phenotypes [35]. Thus, more in-depth, single-cell-level phenotyping and consistent tumor-type categorizations are needed to clarify PTPN7's role in macrophage polarization.

4.3 PTPN7 seems to act as a negative regulator across T cells and macrophages

We carefully reviewed the literature to dissect further the possible pathogenesis mechanism of the PTPN7 mRNA target. Previous literature shows that PTPN7 (also called hematopoietic PTP or HePTP) is highly expressed in T lymphocytes, the same as our data; however, it negatively regulates T-cell receptor (TCR) signaling [36]. Saxena et al. demonstrated that PTPN7 blocks TCR-induced IL-2 promoter activation by inhibiting NFAT/AP-1 [36]. Mechanistically, HePTP dephosphorylates and inactivates ERK2 in stimulated T cells, reducing IL-2 expression [36]. Correspondingly, PTPN7-deficient T cells show enhanced ERK activation and IL-2 production, underscoring its role as a brake on T-cell activation. In innate immune cells, PTPN7 similarly restrains pro-inflammatory signaling. In Song's study, they revealed that PTPN7 deactivates MAPKs (ERK1/2 and p38) in macrophages, decreasing their activation [37]. In LPS-stimulated RAW264.7 macrophages, PTPN7 downregulation is transient, and PTPN7 overexpression strongly suppresses TNF-α production. Conversely, PTPN7 knockdown boosts p38/ERK phosphorylation and raises TNF-α release, establishing PTPN7 as a negative regulator of MAPK-driven inflammation [37]. Recently, Ji X's team also noticed the immune suppressive role of PTPN7 in brain tumors, which mediates macrophage-polarization to M2-like phenotype in a glioma context [24].

4.4 Limitations of this study

Evaluating tissue from the same patients would be ideal for better correlating transcriptome and protein expression. However, our PTPN7 IHC data are derived from tissue microarrays (BioMax, https://www.tissuearray.com/tissue-arrays/Brain/GL1001a) and the RNA-Seq data from TCGA (https://portal.gdc.cancer.gov/), making direct comparisons challenging. We attempted to find matched samples for parallel proteomic analysis but were unsuccessful. Consequently, we individually assessed the correlation of clinical factors (survival, tumor grade, etc.) with PTPN7 protein or mRNA expression. Notably, protein and mRNA data indicate a similar trend of increasing PTPN7 with tumor grade. From a clinical standpoint, routine measurement of PTPN7—whether via mRNA quantification or IHC—could be incorporated into nomograms to refine patient survival predictions.

5 Conclusion

This study underscores the clinical significance of PTPN7 in IDH-wildtype astrocytomas and highlights its immunomodulatory impact in shaping a macrophage-enriched yet T-cell-constrained tumor microenvironment. By leveraging spatial transcriptomics, thorough bioinformatic analyses, and the updated 2021 WHO classification, our findings provide a

rationale for viewing PTPN7 as a prognostic and potentially therapeutic target in gliomas. Future research aimed at dissecting PTPN7's multifaceted role in the tumor microenvironment will aid in developing more effective, precision-oriented treatments for this challenging disease.

Author contributions Manuscript writing: T. Liu and Y.-F.L.; experiments design: Y.-F.L., D.-Y.H.; bioinformatic analysis: Y.-C.L. and Y.-F.L.; experiments and data analysis: Y.-F.L. and P.-C.C.; contribution of reagents/materials/analysis tools: Y.-F.L. and D.-Y.H. All the authors have reviewed and consented to the published edition of the manuscript.

Funding This project received funding from the National Science and Technology Council (111-2314-B-016 -064 -MY3 to Y.-F.L. and 113-2321-B-016 -005 to D.-Y.H.), the Ministry of National Defense Medical Affairs Bureau (MND-MAB-D-113167 to Y.-F.L.), Tri-Service General Hospital (TSGH-E-111269 to T. Liu), and Taipei, Taichung, Kaohsiung Veterans General Hospital, Tri-Service General Hospital, Academia Sinica Joint Research Program (VTA113-T-4-2 to Y.-F.L.).

Data availability Datasets used in this project can be accessed via the TCGA GDC portal (https://portal.gdc.cancer.gov/), CGGA (http://www.cgga.org.cn/), Ivy Glioblastoma Atlas (https://glioblastoma.alleninstitute.org/) and the Single-cell sequencing data from Gene-Expression Omnibus (GEO) databases, GSE131928 (https://www.ncbi.nlm.nih.gov/geo/query/acc.cgi?acc=GSE131928) and GSE89567 (https://www.ncbi.nlm.nih.gov/geo/query/acc.cgi?acc=GSE89567). Glioblastoma Visium dataset (https://www.10xgenomics.com/datasets/human-glioblastoma-whole-transcriptome-analysis-1-standard-1-2-0).

Declarations

Ethics approval and consent to participate This study was approved by the Tri-Service General Hospital Ethics Committee (TSGHIRB No. A202205193), entitled "Brain Tumors Precision Medicine: From Clinical to Genetic and Artificial Intelligence, then Back to Clinical Applications". The research was conducted following the guidelines and regulations outlined by the Tri-Service General Hospital Ethics Committee.

Informed consent Informed consent to participate in this study was obtained from all participants. For the immunohistochemistry (IHC) evaluations, we used a human glioma tissue microarray (GL1001a) from Biomax, Inc., under Biomax's standardized biobanking policies.

Consent for publication Consent to publish was obtained from all participants. If participants were under 18 years of age, consent was obtained from a parent and/or legal guardian.

Competing interests The authors declare no competing interests.

References

1. Ostrom QT, Price M, Neff C, Cioffi G, Waite KA, Kruchko C, et al. CBTRUS statistical report: primary brain and other central nervous system tumors diagnosed in the United States in 2016–2020. Neuro Oncol. 2023;25(12):iv1–99.
2. Louis DN, Ohgaki H, Wiestler OD, Cavenee WK, Burger PC, Jouvet A, et al. The 2007 WHO classification of tumours of the central nervous system. Acta Neuropathol. 2007;114(2):97–109.
3. Louis DN, Perry A, Reifenberger G, von Deimling A, Figarella-Branger D, Cavenee WK, et al. The 2016 World Health Organization Classification of tumors of the central nervous system: a summary. Acta Neuropathol. 2016;131(6):803–20.
4. Louis DN, Perry A, Wesseling P, Brat DJ, Cree IA, Figarella-Branger D, et al. The 2021 WHO classification of tumors of the central nervous system: a summary. Neuro Oncol. 2021;23(8):1231–51.
5. Brat DJ, Aldape K, Colman H, Holland EC, Louis DN, Jenkins RB, et al. cIMPACT-NOW update 3: recommended diagnostic criteria for "Diffuse astrocytic glioma, IDH-wildtype, with molecular features of glioblastoma, WHO grade IV." Acta Neuropathol. 2018;136(5):805–10.
6. Stupp R, Mason WP, van den Bent MJ, Weller M, Fisher B, Taphoorn MJ, et al. Radiotherapy plus concomitant and adjuvant temozolomide for glioblastoma. N Engl J Med. 2005;352(10):987–96.
7. Brat DJ, Aldape K, Colman H, Figrarella-Branger D, Fuller GN, Giannini C, et al. cIMPACT-NOW update 5: recommended grading criteria and terminologies for IDH-mutant astrocytomas. Acta Neuropathol. 2020;139(3):603–8.
8. Brodbelt A, Greenberg D, Winters T, Williams M, Vernon S, Collins VP. Glioblastoma in England: 2007–2011. Eur J Cancer. 2015;51(4):533–42.
9. Ostrom QT, Cote DJ, Ascha M, Kruchko C, Barnholtz-Sloan JS. Adult glioma incidence and survival by race or ethnicity in the United States from 2000 to 2014. JAMA Oncol. 2018;4(9):1254–62.
10. Xie XP, Laks DR, Sun D, Ganbold M, Wang Z, Pedraza AM, et al. Quiescent human glioblastoma cancer stem cells drive tumor initiation, expansion, and recurrence following chemotherapy. Dev Cell. 2022;57(1):32-46.e8.

11. Colardo M, Segatto M, Di Bartolomeo S. Targeting RTK-PI3K-mTOR axis in gliomas: an update. Int J Mol Sci. 2021;22(9):4899.
12. Lin YC, Chang PC, Hueng DY, Huang SM, Li YF. Decoding the prognostic significance of integrator complex subunit 9 (INTS9) in glioma: links to TP53 mutations, E2F signaling, and inflammatory microenvironments. Cancer Cell Int. 2023;23(1):154.
13. Chang PC, Lin YC, Yen HJ, Hueng DY, Huang SM, Li YF. Ancient ubiquitous protein 1 (AUP1) is a prognostic biomarker connected with TP53 mutation and the inflamed microenvironments in glioma. Cancer Cell Int. 2023;23(1):62.
14. Liu T, Liu N-T, Huang Y-C, Hsu W-W, Lin Y-C, Li Y-F. Elucidating the role of SLC4A7 in glioma prognosis: a comprehensive approach combining bioinformatics, single-cell analysis, and tissue validation. J Med Sci. 2023;43(5):202–11.
15. Feng SW, Chang PC, Chen HY, Hueng DY, Li YF, Huang SM. Exploring the mechanism of adjuvant treatment of glioblastoma using temozolomide and metformin. Int J Mol Sci. 2022;23(15):8171.
16. Li YF, Tsai WC, Chou CH, Huang LC, Huang SM, Hueng DY, et al. CKAP2L knockdown exerts antitumor effects by increasing miR-4496 in glioblastoma cell lines. Int J Mol Sci. 2020;22(1):197.
17. Tang Z, Kang B, Li C, Chen T, Zhang Z. GEPIA2: an enhanced web server for large-scale expression profiling and interactive analysis. Nucleic Acids Res. 2019;47(W1):W556–60.
18. Tang Z, Li C, Kang B, Gao G, Li C, Zhang Z. GEPIA: a web server for cancer and normal gene expression profiling and interactive analyses. Nucleic Acids Res. 2017;45(W1):W98-w102.
19. Goldman MJ, Craft B, Hastie M, Repečka K, McDade F, Kamath A, et al. Visualizing and interpreting cancer genomics data via the Xena platform. Nat Biotechnol. 2020;38(6):675–8.
20. Cerami E, Gao J, Dogrusoz U, Gross BE, Sumer SO, Aksoy BA, et al. The cBio cancer genomics portal: an open platform for exploring multidimensional cancer genomics data. Cancer Discov. 2012;2(5):401–4.
21. Babault N, Cordier F, Lafage M, Cockburn J, Haouz A, Prehaud C, et al. Peptides targeting the PDZ domain of PTPN4 are efficient inducers of glioblastoma cell death. Structure. 2011;19(10):1518–24.
22. Cui P, Lian J, Liu Y, Zhang D, Lin Y, Lu L, et al. Pan-cancer analysis of the prognostic and immunological roles of SHP-1/ptpn6. Sci Rep. 2024;14(1):23083.
23. Otani R, Ikegami M, Yamada R, Yajima H, Kawamura S, Shimizu S, et al. PTPN11 variant may be a prognostic indicator of IDH-wildtype glioblastoma in a comprehensive genomic profiling cohort. J Neurooncol. 2023;164(1):221–9.
24. Ji X, Cheng J, Su J, Wen R, Zhang Q, Liu G, et al. PTPN7 mediates macrophage-polarization and determines immunotherapy in gliomas: a single-cell sequencing analysis. Environ Toxicol. 2024;39(10):4562–80.
25. Zou F, Rao T, Chen W, Song T, Li T, Hu W, et al. DUSP2 affects bladder cancer prognosis by down-regulating MEK/ERK and P38 MAPK signaling pathways through PTPN7. Cell Signal. 2023;112: 110893.
26. Balasundaram A, Doss GPC. Deciphering the impact of rare missense variants in EGFR-TKI-resistant non-small-cell lung cancer through whole exome sequencing: a computational approach. ACS Omega. 2024;9(14):16288–302.
27. Liu Y, Zhang J, Du Z, Huang J, Cheng Y, Yi W, et al. Comprehensive analysis of PTPN family expression and prognosis in acute myeloid leukemia. Front Genet. 2022;13:1087938.
28. Zhang Y, Chen Y, Shi L, Li J, Wan W, Li B, et al. Extracellular vesicles microRNA-592 of melanoma stem cells promotes metastasis through activation of MAPK/ERK signaling pathway by targeting PTPN7 in non-stemness melanoma cells. Cell Death Discov. 2022;8(1):428.
29. Wang F, Wang X, Liu L, Deng S, Ji W, Liu Y, et al. Comprehensive analysis of PTPN gene family revealing PTPN7 as a novel biomarker for immunohot tumors in breast cancer. Front Genet. 2022;13: 981603.
30. Le T, Phan T, Pham M, Tran D, Lam L, Nguyen T, et al. BBrowser: making single-cell data easily accessible. bioRxiv : the preprint server for biology. 2020:2020.12.11.414136.
31. Subramanian A, Tamayo P, Mootha VK, Mukherjee S, Ebert BL, Gillette MA, et al. Gene set enrichment analysis: a knowledge-based approach for interpreting genome-wide expression profiles. Proc Natl Acad Sci U S A. 2005;102(43):15545–50.
32. Varn FS, Johnson KC, Martinek J, Huse JT, Nasrallah MP, Wesseling P, et al. Glioma progression is shaped by genetic evolution and microenvironment interactions. Cell. 2022;185(12):2184-99.e16.
33. Chen B, Khodadoust MS, Liu CL, Newman AM, Alizadeh AA. Profiling Tumor Infiltrating Immune Cells with CIBERSORT. Methods Mol Biol. 2018;1711:243–59.
34. Zarodniuk M, Steele A, Lu X, Li J, Datta M. Pan-cancer transcriptomic analysis of CNS tumor stroma identifies a population of perivascular fibroblasts that predict poor immunotherapy response in glioblastoma patients. Res Sq. 2023. https://doi.org/10.21203/rs.3.rs-2931886/v1.
35. Abdelfattah N, Kumar P, Wang C, Leu JS, Flynn WF, Gao R, et al. Single-cell analysis of human glioma and immune cells identifies S100A4 as an immunotherapy target. Nat Commun. 2022;13(1):767.
36. Saxena M, Williams S, Gilman J, Mustelin T. Negative regulation of T cell antigen receptor signal transduction by hematopoietic tyrosine phosphatase (HePTP). J Biol Chem. 1998;273(25):15340–4.
37. Seo H, Lee IS, Park JE, Park SG, Lee DH, Park BC, et al. Role of protein tyrosine phosphatase non-receptor type 7 in the regulation of TNF-α production in RAW 264.7 macrophages. PLoS ONE. 2013;8(11): e78776.